Journal of Materials Science and Engineering A 14 (7-9) (2024) 78-85
doi: 10.17265/2161-6213/2024.7-9.003

Gradient-Resistivity 3D Current Collectors for Lithium Dendrite Suppression

Changmyeon Lee[1,2], Jun-mi Jeon[2], Hideo Honma[3], Osamu Takaic[3] and Joo-Hyong Noh[1,3]

1. Graduate School of Engineering, Kanto Gakuin University, Yokohama 236-8501, Japan

2. Industrial Components R&D Department, Korea Institute of Industrial Technology, Incheon 21996, South Korea

3. Materials and Surface Engineering Research Institute, Kanto Gakuin University, Yokohama 236-8501, Japan

Abstract: Lithium metal batteries provide high theoretical energy density and storage capacity but suffer from performance degradation and safety issues due to lithium dendrite formation. This research designed a resistivity gradient structure based on a 3D porous current collector to inhibit dendrite growth. Through a UV (ultraviolet) inactivation process, catalyst formation at the upper layers was suppressed, limiting the upper copper plating and enhancing plating toward the lower part during the electroless plating stage. Subsequently, electroplating was performed to increase the copper thickness. Experimental results showed that this gradient-resistivity current collector minimized the surface lithium deposition, which blocks pores. The charge-discharge stability evaluation demonstrated that batteries using this gradient structure exhibited higher stability and improved performance in full-cell and symmetrical-cell tests. This study presents significant technological progress toward commercializing lithium metal batteries.

Key words: 3D porous current collectors, resistivity gradient, lithium metal batteries, electroless plating, UV-catalyst inactivation.

1. Introduction

LMBs (lithium metal batteries), due to their high energy density of 3,860 mAh/g and low electrochemical potential of -3.04 V vs. SHE, are considered a promising next-generation energy storage system [1-9]. However, during charge-discharge cycles, irregular lithium deposition can lead to dendrite formation, significantly degrading performance and posing severe safety risks. This issue is exacerbated in high-current-density environments, leading to potential short circuits or even explosions under severe conditions [7, 10-14].

Various studies have been conducted to resolve this issue, with significant attention on utilizing 3D porous current collectors to reduce current density and promote uniform lithium deposition [15-18]. Yang et al. [16] reported that sub-micron structured 3D current collectors effectively suppressed the growth of lithium dendrites, maintaining superior electrochemical performance without short circuits for more than 600 h. Cipollone et al. [17] demonstrated that the use of a 3D copper nanowire grid structure enhanced the interface stability of the lithium metal anode, inhibiting dendrite growth and maximizing battery performance. Additionally, Park et al. Ref. [18] showed that a mechanically calendared optimized 3D structure of Cu-CNT (Cu-carbon nanotube) composites improved the uniformity of lithium plating, maintaining long-term cycle performance.

While these studies based on 3D structures mark significant advancements in suppressing lithium dendrite growth and enhancing battery performance, several limitations still exist. Primarily, conventional 3D porous structures are challenged by complex manufacturing processes and high production costs, which hinder their commercialization [15]. Furthermore, the difficulty in uniformly controlling pore sizes complicates the scalability to larger structures. Particularly, the phenomenon of top-plating, where lithium preferentially plates on the surface facing the cathode, blocking the pores and thus restricting internal filling, can accelerate dendrite

Corresponding author: Changmyeon Lee, Doctoral student, research field: surface treatment.

growth, leading to concentrated lithium deposition at the top [19].

This study aimed to overcome these limitations by developing a more cost-effective and manufacturable gradient-resistivity 3D current collector. A fiber-based porous structure was designed, suitable for large-scale production. To induce uniform lithium filling within the collector, a UV (ultraviolet) inactivation process controlled the plating thickness by suppressing catalyst formation at the upper layers and promoting increased plating toward the bottom, establishing a resistivity gradient. This method was evaluated to determine its effectiveness in suppressing dendrite growth and enhancing charge-discharge performance of lithium metal batteries.

2. Experimental Procedures

A porous commercial fiber (Hirose, micro-fiber) was employed as the substrate for creating 3D current collectors. Initially, these fibers were subjected to a surface modification process using an atmospheric pressure plasma (iREV, API) to remove contaminants and enhance the surface's reactivity, essential for subsequent chemical treatments. The fibers were then immersed in a Sn^{2+} ion solution for 1 min for sensitization, preparing the surface for the palladium catalyst deposition. Following this, the fibers were briefly dipped in a palladium solution for 20 s, allowing the Sn^{2+} ions absorbed on the surface to react with Pd^{2+} ions, forming Pd^{0} catalytic sites by reducing Pd^{2+} to Pd^{0} via a redox reaction.

To establish a gradient of resistivity in the collectors, after sensitization, the fibers were exposed to UV light with a wavelength of 365 nm for 1 min. This UV exposure altered the surface properties along the length of the fibers, controlling the catalyst deposition process. Post UV exposure, the fibers were immersed again in the palladium solution to ensure sufficient catalytic activity was achieved for effective copper deposition. The final stage involved immersing the fibers in an electroless copper plating solution for 10 min, which deposited a uniform copper layer across the catalyzed surfaces.

The completed 3D collectors were then used for lithium metal deposition. A custom split cell setup with a load cell was employed to control uniaxial pressure during the electroplating at a controlled current density. Lithium metal served as the counter electrode, and the fabricated 3D collector acted as the working electrode, with a polypropylene separator in between. Lithium electroplating and cycling tests were conducted using a 3M lithium bis(trifluoromethanesulfonyl)imide (LiTFSI) in dimethyl ether (DME) solution, enhanced with 1% lithium nitrate ($LiNO_3$) and 3% fluoroethylene carbonate (FEC), maintained in a glove box under an argon atmosphere with moisture and oxygen levels below 0.5 ppm.

After the electroplating process, the electrodeposited lithium on the 3D collectors was characterized using a SEM (scanning electron microscope, Thermo Fisher Scientific, Sirion TM) and further cross-sectional analysis performed using a FIB system (focused ion beam, Thermo Fisher Scientific, NOVA-600).

The electrochemical performance and cycle stability of the deposited lithium were evaluated using a 2032 coin-type cell setup, with the 3D collector as the anode and a copper counter electrode. The cycling tests were conducted using a WBCS3000 battery test system, with a Li|NCM622 full cell configuration to further assess the operational stability and Coulombic efficiency. The NCM622 cathode was prepared by slurry coating onto an aluminum collector, mixing NCM622 active material, conductive carbon (Super P), and binder (polyvinylidene fluoride, PVDF) in N-methyl-2-pyrrolidone (NMP) solvent, dried and compressed to the desired thickness. Cycling of the full cells was performed between 2.5 V and 4.2 V at a rate of 0.5 C to evaluate the long-term stability and capacity retention of the lithium metal electrodes with the gradient-resistivity 3D collectors.

3. Results and Discussion

A 3D current collector was fabricated by metallizing

fibers with a porosity of 85.30% and a thickness of approximately 80 μm using an electroless copper plating method. Initially, the fiber surface was modified using a NaOH alkaline solution. Subsequently, the fibers were immersed in a Sn^{2+} ion solution for sensitization treatment, followed by immersion in an activation solution containing Pd^{2+} ions. During this process, the Sn^{2+} ions adsorbed on the fiber surface reacted with Pd^{2+} ions according to the reaction below, oxidizing to Sn^{4+}. This reaction released two electrons that reduced the Pd^{2+} ions to Pd^0, ultimately forming a Pd catalyst.

$$Sn^{2+} + Pd^{2+} \rightarrow Sn^{4+} + Pd^0 \quad (1)$$

The activated fibers were immersed in an electroless copper plating solution for 10 min to confer conductivity. Fig. 1 shows the fiber surface before and after electroless plating observed by SEM. Image analysis indicated that the plating was uniformly applied, with an increase in thickness of about 1.73 μm compared to before plating. After metallization, the final porosity was measured at 77.98%. Using Eq. (2) assuming the fibers as cylindrical, the calculated average copper coating thickness was 1.76 μm, which showed a similar value to the SEM analysis results. This result validates the accuracy of thickness measurement by SEM and provides quantitative verification of the process.

$$t_{plating} = D\left(\sqrt{\frac{1-P_f}{1-P_i}} - 1\right) \quad (2)$$

This fiber-based 3D collector was then filled with lithium metal using an electrochemical method. The anode was the 3D collector, and the cathode was a lithium metal foil with a thickness of 200 μm, using a 25 μm thick Cellguard 2400 PP separator. The electrolyte consisted of 3 M LiTFSI and DME as the base, with 1% $LiNO_3$ and 3% FEC added. The lithium charging process was conducted at a constant current of 1 mA/cm², and a total of 8 mAh/cm² capacity was filled at the anode. The estimated thickness of the filled lithium, based on the density of lithium metal (0.534 g/cm³), was calculated to be 38.8 μm through Eq. (3). Considering the initial thickness of 80 μm and a porosity of 79.53%, the internal void space within the fibers was about 63.62 μm, indicating that the filled lithium appropriately filled the space without overflowing.

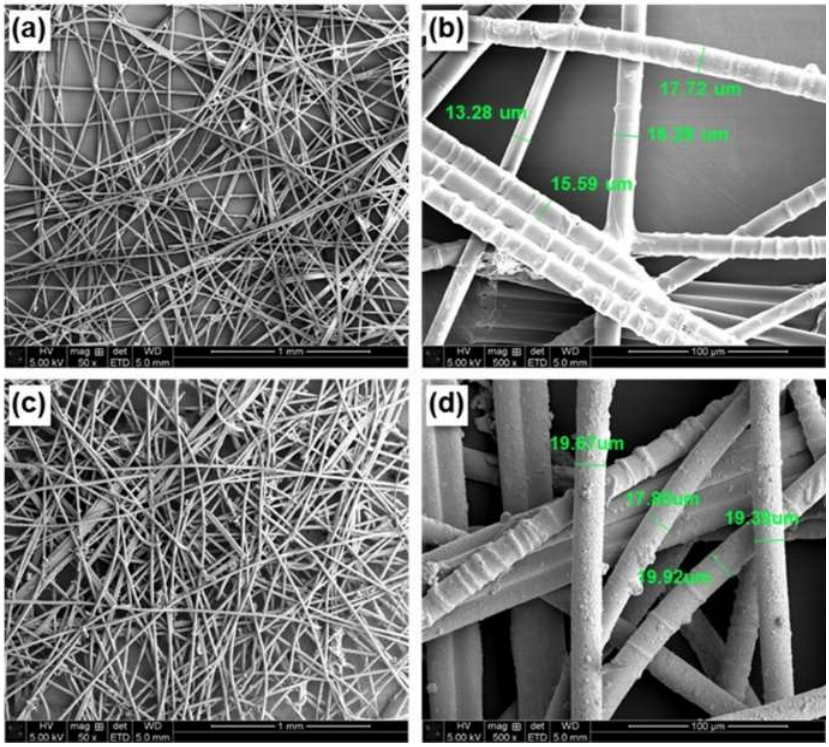

Fig. 1 SEM images of fibers before and after electroless copper plating: (a) pre-plating, (b) magnified view showing 15.72 μm thickness, (c) post-plating, (d) magnified view with 19.18 μm thickness.

$$t_{plating} = \frac{M \cdot I \cdot t}{n \cdot F \cdot d} \quad (3)$$

Fig. 2a presents the voltage changes as a function of areal capacity during lithium plating at a current density of 1 mA/cm² over an 8-hour period. This graph can be divided into three sections:

Section 1: The voltage changes significantly initially, reflecting the rapid formation and growth of lithium nuclei on the collector surface until a continuous lithium film is formed.

Section 2: The voltage continues to decrease, which can occur due to the phenomenon of top-plating mentioned in previous studies, making ion transfer inside more difficult as the actual plating surface area decreases over time, increasing the effective current density and leading to an increase in overpotential.

Section 3: The voltage gradually converges to about -0.024 V. This stabilization of voltage suggests that additional lithium plating is predominantly occurring on the surface, indicating that further internal lithium plating is virtually not happening.

To directly verify whether the top-plating phenomenon occurred, the lithium filling behavior of the 3D collector was observed under SEM. Figs. 2b and 2c show the top (near the cathode) and bottom (opposite the cathode) surfaces of the 3D collector after lithium filling. In Fig. 2b, lithium was predominantly plated on the top surface, forming a thick layer of lithium, which obscured the fiber structure by lithium dendrites. Conversely, Fig. 2c shows relatively more empty spaces at the bottom surface, indicating insufficient internal lithium filling. These observations confirm that the top-plating phenomenon actually occurred during the lithium filling process.

Two approaches were considered to alleviate the top-plating phenomenon. The first involves applying a gradient to the pore sizes of the fibers, placing larger pores at the top and smaller ones at the bottom,

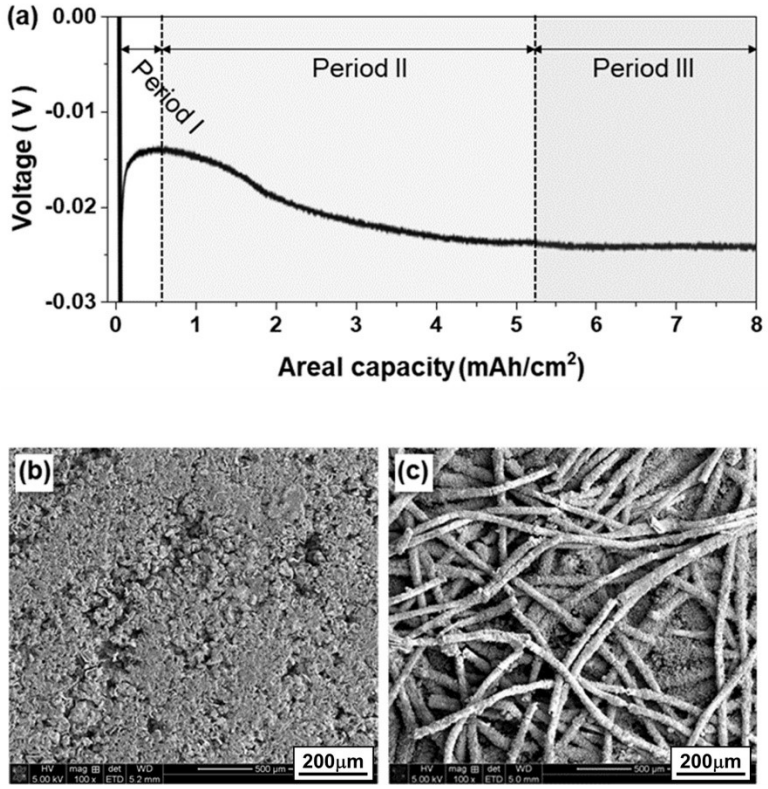

Fig. 2 (a) Voltage vs. areal capacity for lithium plating at 1 mA/cm² up to 8 mAh/cm²; (b) and (c) SEM images of the 3D collector's top (b) and bottom (c) surfaces post-lithium filling.

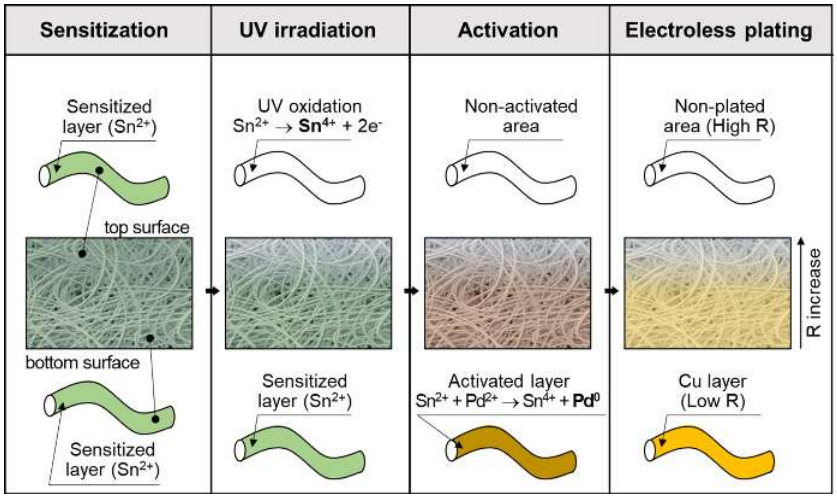

Fig. 3 Schematic illustration of the UV-assisted electroless plating process showing sensitization, UV irradiation, activation, and plating steps, which form an electrical resistance gradient across the fiber depth.

ensuring that even if plating occurs preferentially at the top, it does not block the pores. However, the continuous production of fibers with various pore sizes is technically challenging and results in a reduction in porosity at the bottom, consequently increasing the weight and volume of the collector required to adequately fill with lithium, leading to a decrease in battery energy density. As an alternative, this study opted for the second approach of setting a gradient in electrical resistance across the depth of the collector. By increasing the resistance at the top and decreasing it at the bottom, lithium is more smoothly filled from the bottom, effectively suppressing top-plating.

To implement this gradient in electrical resistance, a UV-assisted electroless plating thickness control technique was applied. This process is detailed in Fig. 3. Initially, surface-modified porous fibers underwent a sensitizing process that adsorbed Sn^{2+} ions, followed by appropriate UV irradiation. UV irradiation plays a crucial role in oxidizing adsorbed Sn^{2+} ions to Sn^{4+}, particularly under strong UV exposure near the top surface where most Sn^{2+} is oxidized. Since oxidized Sn^{4+} ions cannot release electrons to reduce Pd^{2+} to metallic Pd^{0} in the activation process, catalyst formation is hindered at the top. In contrast, Sn^{2+} remains at the relatively less exposed bottom surface, where Pd catalyst forms upon immersion in the activation solution. This method increases the concentration of Pd catalyst formation from top to bottom, consequently increasing the thickness of the electroless plating and forming an electrical resistance gradient along the depth of the collector.

The effectiveness of the manufactured gradient-resistivity 3D collector was evaluated through lithium filling experiments. Fig. 4a shows the voltage-time graph obtained during lithium filling, with the results for the gradient-resistivity 3D collector displayed in black and those for the uniform-resistivity 3D collector in grey. Notably, the gradient-resistivity 3D collector does not show a significant increase in resistance even after the formation of a lithium film, indicating that internal lithium filling was proceeding smoothly. However, a slight decrease in voltage was observed, likely due to a reduction in surface area during the filling process.

To directly verify the effect of top-plating suppression, lithium filling behavior was observed under SEM after plating. Figs. 4b and 4c show the top and bottom surfaces of the gradient-resistivity 3D collector after lithium filling. These images confirm the absence of top-plating on both surfaces, and the fibers inside are sufficiently filled, particularly visible on the top surface where un-plated fibers are exposed. These results suggest that internal lithium filling was effectively carried out, proving that the gradient-resistivity 3D collector plays a crucial role in

suppressing top-plating during the lithium plating process.

As shown in Fig. 5, half-cell tests utilizing both gradient-resistivity and uniform-resistivity 3D collectors, each filled with 8 mAh/cm² of lithium, demonstrated the superior stability of the gradient-resistivity collector, maintaining stable charge-discharge performance over approximately 250 cycles. In contrast, the uniform-resistivity collector exhibited a significant drop in Coulombic efficiency, ceasing operation around 116 cycles.

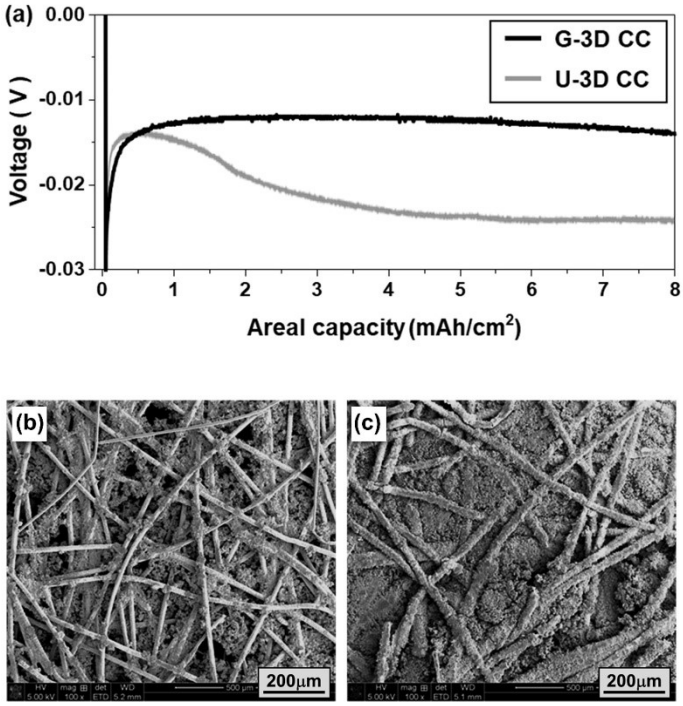

Fig. 4 (a) Voltage vs. areal capacity for gradient-resistivity (black) and uniform-resistivity (gray) collectors; (b) and (c) SEM images of the top (b) and bottom (c) surfaces post-lithium filling.

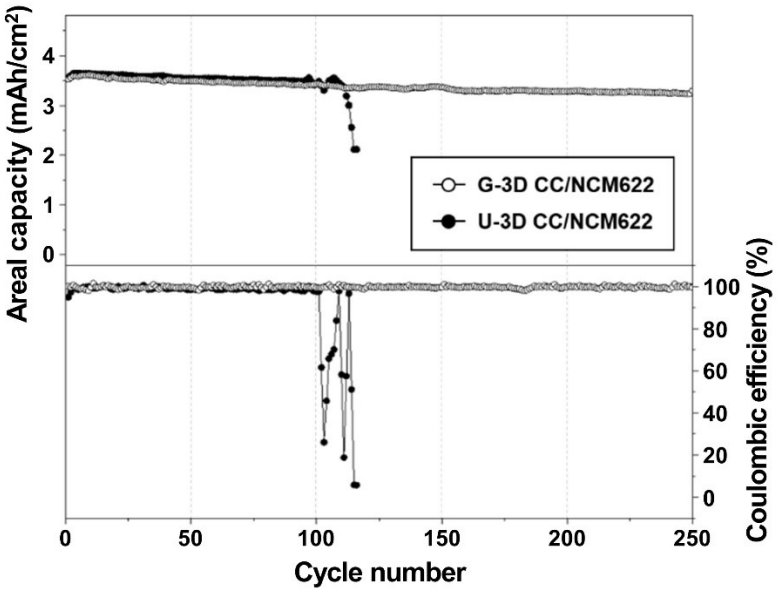

Fig. 5 Half-cell tests comparing gradient-resistivity and uniform-resistivity 3D collectors, highlighting superior stability of the gradient-resistivity design with stable charge-discharge over 250 cycles versus 116 cycles for the uniform-resistivity collector.

These research results confirm that suppressing top-plating through a gradient in electrical resistance contributes to enhancing the stability of lithium metal batteries. However, additional research on variables such as UV exposure time and plating thickness optimization is needed. Such detailed studies can provide clues to the mass production potential of high-performance and highly stable 3D collectors using an economically feasible and easily manufacturable method. This contributes not only to the advancement of sustainable battery technology but also plays a crucial role in maximizing the efficiency of electric vehicles and energy storage systems.

4. Conclusions

This study developed a gradient-resistivity structure based on 3D porous current collectors to address the performance degradation and safety issues of lithium metal batteries. By deactivating the catalyst formation at the top through UV irradiation and progressively increasing the plating thickness toward the bottom, this approach promotes uniform lithium ion deposition and optimizes internal lithium filling. This method minimizes the top-plating phenomenon, where lithium preferentially plates on the upper surface blocking pores, while maintaining the overall porosity of the 3D current collector, enabling efficient lithium plating.

The evaluation of charge-discharge stability demonstrated that the gradient-resistivity 3D collector exhibits higher cycle stability and improved Coulombic efficiency compared to the uniform-resistivity 3D collector. This confirms that the gradient-resistivity structure effectively suppresses dendrite growth and induces a uniform distribution of lithium. Furthermore, the use of gradient-resistivity 3D current collectors suggests a positive impact on the overall performance and stability enhancement of lithium metal batteries.

Acknowledgments

This work was supported by the National Research Foundation of Korea (NRF) grant funded by the Korea government (MSIT) (No. 2022M3J1A1085403). This research was funded by the Korea Institute of Industrial Technology as “Development of root technology for multi-product flexible production” (KITECH EO-24-0009).

References

[1] Li, Q., Zhu, S., and Lu, Y. 2017. “3D Porous Cu Current Collector/Li-Metal Composite Anode for Stable Lithium-Metal Batteries.” *Adv. Funct. Mater*. 27: 1606422.

[2] Liu, H., Wang, E., Zhang, Q., Ren, Y., Guo, X., Wang, L., Li, G., and Yu, H. 2019. “Unique 3D Nanoporous/Macroporous Structure Cu Current Collector for Dendrite-Free Lithium Deposition.” *Energy Storage Materials* 17: 253-9.

[3] Schmuch, R., Wagner, R., Hörpel, G., Placke, T., and Winter, M. 2018. “Performance and Cost of Materials for Lithium-Based Rechargeable Automotive Batteries.” *Nature Energy* 3: 267-78.

[4] Manthiram, A. 2020. “A Reflection on Lithium-Ion Battery Cathode Chemistry.” *Nat. Commun*. 11: 1550.

[5] Dresselhaus, M. S., and Thomas, I. 2001. “Alternative Energy Technologies.” *Nature* 414: 332-7.

[6] Goodenough, J. B., and Kim, Y. 2010. “Challenges for Rechargeable Li Batteries.” *Chemistry of Materials* 22: 587-603.

[7] Liu, B., Zhang, J.-G., and Xu, W. 2018. “Advancing Lithium Metal Batteries.” *Joule* 2: 833-45.

[8] Xu, W., Wang, J., Ding, F., Chen, X., Nasybulin, E., Zhang, Y., and Zhang, J.-G. 2014. “Lithium Metal Anodes for Rechargeable Batteries.” *Energy Environ. Sci*. 7: 513-37.

[9] Lin, D., Liu, Y., and Cui, Y. 2017. “Reviving the Lithium Metal Anode for High-Energy Batteries.” *Nature Nanotechnol* 12: 194-206.

[10] Lu, Y., Tu, Z., and Archer, L. A. 2014. “Stable Lithium Electrodeposition in Liquid and Nanoporous Solid Electrolytes.” Nature Materials 13: 961-9.

[11] Zhang, J.-G., Xu, W., and Henderson, W. A. 2017. *Lithium Metal Anodes and Rechargeable Lithium Metal Batteries.* New York: Springer International.

[12] Cao, R., Xu, W., Lv, D., Xiao, J., and Zhang, J. G. 2015 “Anodes for Rechargeable Lithium-Sulfur Batteries.” *Adv. Energy Mater*. 5: 1402273.

[13] Li, N. W., Shi, Y., Yin, Y. X., Zeng, X. X., Li, J. Y., Li, C. J., Wan, L. J., Wen, R., and Guo, Y. G. 2018. “A Flexible Solid Electrolyte Interphase Layer for Long-Life Lithium Metal Anodes.” *Angew. Chem., Int. Ed*. 57: 1505-9.

[14] Wang, S. H., Yin, Y. X., Zuo, T. T., Dong, W., Li, J. Y., Shi, J. L., Zhang, C. H., Li, N. W., Li, C. J., and Guo, Y.

G. 2017. “Stable Li Metal Anodes via Regulating Lithium Plating/Stripping in Vertically Aligned Microchannels.” *Adv. Mater.* 29: 1703729.

[15] Park, S. H., Jun, D. Y., Lee, G. H., Lee, S. G., Jung, J. E., Bae, K. Y., Son, S., and Lee, Y. J. 2022. “Designing 3D Anode Based on Pore-Size-Dependent Li Deposition Behavior for Reversible Li-Free All-Solid-State Batteries.” *Adv. Sci.* 9: 2203130.

[16] Yang, C.-P., Yin, Y.-X., Zhang, S.-F., Li, N.-W., and Guo, Y.-G. 2015. “Accommodating Lithium into 3D Current Collectors with a Submicron Skeleton towards Long-Life Lithium Metal Anodes.” *Nat. Commun*. 6 (1): 1-9.

[17] Cipollone, D., Yang, H., Yang, F., Bright, J., Liu, B., Winch, N., Sierros, K. A., and Wu, N. 2021. “3D Printing of an Anode Scaffold for Lithium Batteries Guided by Mixture Design-Based Sequential Learning.” *J. Mater. Process. Technol*. 295: 117159.

[18] Park, S. K., Copic, D., Zhao, T., Rutkowska, A., Wen, B., Sanders, K., He, R., Kim, H. K., and Volder, M. D. 2023. “3D Porous Cu-Composites for Stable Li-Metal Battery Anodes.” *ACS Nano*. 17: 14658-66.

[19] Kim, D.-H., Lee, M.-H, Kim, B. G., Lee, S.-M., and Choi, J.-H. 2020. “Porosity Controlled Carbon-Based 3D Anode for Lithium Metal Batteries by a Slurry Based Process.” *Chem. Commun. (Camb)*. 56 (85): 13040-3. doi: 10.1039/d0cc05141a.